

Improving Materials for Compact Thermal Energy Storage: Two Case Studies on Tailor-Made Polyalcohol Mixtures (PCMs) and Composites of Chlorides Confined in Gamma-Alumina or Silica-PEG (TCMs)

Alenka Ristić, Suzana Mal, Nataša Zabukovec Logar, Elise Bérut, Laurence Bois, Jonathan Outin, Michel Ondarts, Nolwenn Le Pierrès, Ángel Serrano, Mikel Durán, et al.

▶ **To cite this version:**

Alenka Ristić, Suzana Mal, Nataša Zabukovec Logar, Elise Bérut, Laurence Bois, et al.. Improving Materials for Compact Thermal Energy Storage: Two Case Studies on Tailor-Made Polyalcohol Mixtures (PCMs) and Composites of Chlorides Confined in Gamma-Alumina or Silica-PEG (TCMs). ACS Applied Energy Materials, 2024, 7 (20), pp.9242-9254. ⟨10.1021/acsaem.4c01702⟩. ⟨hal-04768698⟩

HAL Id: hal-04768698

https://hal.science/hal-04768698v1

Submitted on 6 Nov 2024

HAL is a multi-disciplinary open access archive for the deposit and dissemination of scientific research documents, whether they are published or not. The documents may come from teaching and research institutions in France or abroad, or from public or private research centers.

L'archive ouverte pluridisciplinaire **HAL**, est destinée au dépôt et à la diffusion de documents scientifiques de niveau recherche, publiés ou non, émanant des établissements d'enseignement et de recherche français ou étrangers, des laboratoires publics ou privés.



HAL Authorization

Improving materials for compact thermal energy storage: Tailoring PCM and TCM properties

Alenka Ristić[1*], Suzana Mal[1], Nataša Zabukovec Logar[1,2], Elise Bérut[3], Laurence Bois[4], Jonathan Outin[3], Michel Ondarts[3], Nolwenn Le Pierrès[3*], Ángel Serrano[5*], Mikel Durán[5,6], Sergio Santos[7], Elena Palomo Del Barrio[5,8], Stefania Doppiu[5*]

[1] *National Institute of Chemistry, Department of Inorganic Chemistry and Technology, Hajdrihova 19, SI-1000 Ljubljana, Slovenia*
[2] *University of Nova Gorica, SI-5000 Nova Gorica, Slovenia*
[3] *LOCIE Laboratory, UMR 5271, Université Savoie Mont-Blanc, CNRS, 73370 Le Bourget-du-Lac, France*
[4] *LMI Laboratory, UMR 5615, Université Claude Bernard Lyon 1, CNRS, 69622 Villeurbanne, France*
[5] *Centre for Cooperative Research on Alternative Energies (CIC energiGUNE), Basque Research and Technology Alliance (BRTA), Alava Technology Park, Albert Einstein 48, 01510 Vitoria-Gasteiz, Spain*
[6] *University of the Basque Country (UPV/EHU), Plaza Europa 1, 20018 Donostia-San Sebastián, Spain.*
[7] *TECNALIA Research & Innovation, Basque Research and Technology Alliance (BRTA), Alava Technology Park, Leonardo Da Vinci 11, 01510 Vitoria-Gasteiz, Spain*
[8] *Ikerbasque, Basque Foundation for Science, 48013 Bilbao, Spain*

*Corresponding authors:
Nolwenn Le Pierrès: nolwenn.le-pierres@univ-smb.fr
Alenka Ristić: alenka.ristic@ki.si
Angel Serrano: aserrano@cicenergigune.com
Stefania Doppiu: sdoppiu@cicenergigune.com

Abstract: This article discusses strategies for enhancing the thermophysical properties of phase change materials (PCMs) and thermochemical materials (TCMs) for thermal energy storage (TES) and, in particular, space heating applications. The focus is on increasing energy storage density of PCMs and TCMs, tuning the working temperatures of organic plastic crystals) and increasing the durability of TCM composites. Two case studies on tailored materials are presented, one on PCMs and the other on TCMs. The first case study explores solid-solid PCMs such as pentaerythritol (PE) and pentaglycerine (PG). The research emphasizes the synthesis and thermal properties of the PE:PG binary system with the goal of achieving a discharging temperature of 140 ºC and an optimized latent heat of 177 $J \cdot g^{-1}$. This temperature is particularly relevant as current PCM options within this temperature range struggle with stability. This tailored system exhibits promising thermal characteristics, surpassing other commercial PCMs in both heat storage density (250 $MJ \cdot m^3$) and thermal conductivity (0.59 $W \cdot m^{-1} \cdot K^{-1}$). The second case study focuses on the development and testing of two different types of TCM composites. The first type of composites is formed of a granulated mesoporous γ-alumina matrix (having a high density, 5 nm mesopores and a good structural stability), and LiCl, $CaCl_2$ or $MgCl_2$. The theoretical heat storage density was

determined in appropriate conditions for space heating (adsorption at 30 °C under a water vapor pressure of 12.5 mbar, and desorption at 100 °C). The composites were ranked as follows: γ-alumina-10LiCl (711 kWh.m^{-3}), γ-alumina-10$CaCl_2$ (700 kWh.m^{-3}) and γ-alumina-7$MgCl_2$ (334 kWh.m^{-3}). The second type of composites is made of a silica-PEG matrix and of $MgCl_2$ or $CaCl_2$. Experiments in an open lab-scale reactor demonstrated that the silica-PEG matrix effectively stabilized hydrated 25 wt.% $MgCl_2$ and 36 wt.% $CaCl_2$. Among these, the composite with 25 wt.% of $MgCl_2$ showed the best performance, with an average heat storage density of 216 kWh.m^{-3} (adsorption at 30 °C under a water vapor pressure of 12.1 mbar, and desorption at 130 °C).

Keywords: Low temperature compact thermal energy storage, phase change materials, thermochemical materials, energy storage density, tailor-made materials

Introduction

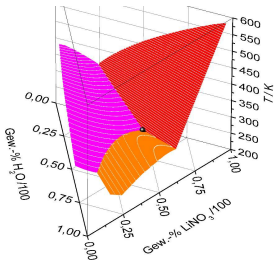
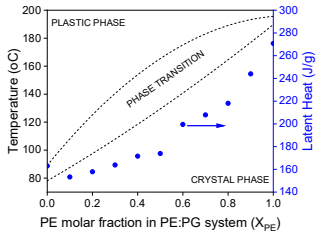
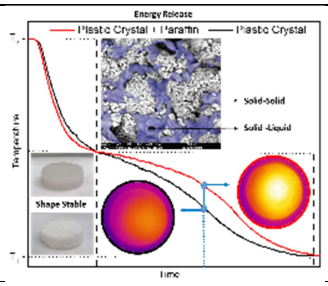
To promote the efficient use and penetration of renewable energies, an energy storage medium is paramount to overcome the problem of intermittency. This provides flexibility to the power grid enabling the efficient management of the energy sources [1, 2]. Energy storage systems can be designed based on different principles depending on the type of application and the desired energy conversion (e.g., power-to-heat, power-to-heat-to-power and power-to-X, where X represents a valuable fuel like hydrogen, syngas, etc.) [3-7]. In this context, thermal energy storage offers a viable solution for managing energy resources according to the requirement of specific application fields [8-10]. This underscores the need for highly efficient, low-cost and compact thermal energy storage (TES) systems than can be integrated into the targeted applications. The success of this depends on both the rational design of the TES system components and the identification of suitable materials and processes that meet the application requirements [11-16].

Thermal energy storage can be achieved using different types of materials, with a wide variety of chemical compositions and operational temperature ranges. Generally, organic materials are preferred for low temperature applications, inorganic salts/porous solids are suitable for low to high temperatures and metals/metal (hydr)oxides for high and extremely high temperatures. The main goal is to design TES materials that significantly improve the efficiency of TES systems, thereby reducing costs. In this context, the development of materials with the highest energy densities is essential for compact storage solutions. Additionally, simplifying the storage concept and TES system design is crucial. This can be accomplished by using solid-solid based PCMs, encapsulation and shape stabilization techniques. These techniques aim at eliminating the need for heat exchangers and the challenges associated with liquid phases in solid-liquid PCMs. Such approaches can also address potential compatibility issues between the TES material, heat transfer fluid and containment materials [17].

The study and optimization of TES materials can follow different paths depending on the type of material (PCMs, TMCs) and the specific objectives. In general, this involves i) developing materials with the highest possible enthalpies (reaction, sorption or transition) and tailored temperatures, ii) adjusting the thermophysical properties [18] such as thermal conductivity and specific heat and iii) ensuring process reversibility under the selected conditions such as mitigating subcooling, preventing degradation and increasing durability. These general targets are the focus of the IEA/SHC Task67/40 "*Compact Thermal Energy*

Storage Materials within Components within Systems" [19] were several experts on TES materials belonging to different institutions in Europe are participating. The current work aims to establish guidelines for materials optimization. In this context, increasing energy density of PCMs and TCMs, along with ensuring long-term stability is key aspect that could significantly enhance the efficiency of TES systems. Table 1 presents some selected examples of PCMs with the associated optimization strategies and corresponding references.

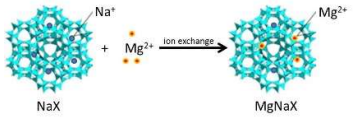
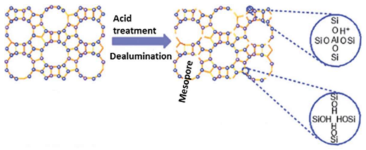
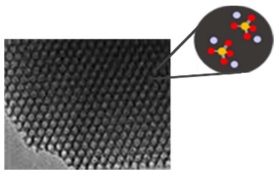
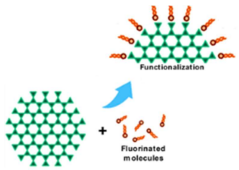
Table 1. Examples of PCMs optimization strategies

	Type of materials (examples)	Type of transition	Optimization route	Expected outcomes
PCMs	Organic PCMs, Fatty acids, Esters, Paraffins, Salt hydrates, Natural oils	S-L	New formulations	- Latent heat enhancement - Tuning temperatures - Subcooling mitigation
	Novel ternary mixtures of salt hydrates, salts, and water	S-L		Solid-liquid phase diagrams: Theoretical prediction and experimental determination - Latent heat enhancement - Tuning temperatures
	Plastic Crystals, Ionic Plastic Crystals [20, 21]	S-S		New solid-solid molecule design - Latent heat enhancement - Tuning temperatures
	S-L and S-S PCM Hybrid PCM-TCM concept: S-L and S-S PCM as a TCM (salt hydrates) matrix [22-24]	Combined composites		New materials/mixture; Thermophysical properties improvement - Latent heat enhancement - Shape stabilization - Solving compatibility issues

For PCMs, increasing the transition enthalpy can be pursued through different approaches such as new material formulations based on binary, ternary and multiple phases or hybrid systems (PCM/TCM). In some cases, this can also offer additional advantages such as shape stabilization, specifically when one of the components undergoes a highly energetic solid-solid phase transition. In these cases, similar transition temperatures and ensuring chemical compatibility between the materials are essential prerequisites for the successful application of this strategy.

Table 2 provides some selected examples of TCMs with their corresponding optimization strategies and the relevant references. The optimization strategies for TCMs include modifying the crystal structure by atomic substitution [32, 37, 44] leading to a modification of the thermodynamic properties of the material (temperature and reaction/sorption enthalpy). For porous materials involved in sorption-based processes, the increase of the sorption enthalpy can be achieved by functionalizing the porous structure with selected atoms/molecules. The aim is to enhance the affinity of the material towards water molecules (stronger interactions between the sorbent surface and water). Another key involves combining sorption processes and chemical reactions by synthesizing composites where a porous material is filled with a salt hydrate (chemical reaction, for example hydration-dehydration).

Table 2. TCMs optimization strategies

	Type of materials (examples)	Type of reaction/ process	Optimization route	Expected outcome
TCMs	Oxides, Hydroxides Inorganic and Organic Salts Hierarchical Zeolites, Ion exchanged zeolites, Hierarchical aluminophosphates, MOFs, ZIFs [25- 36]	Hydration, Adsorption	Doping  Ion exchange of zeolites  Dealumination	From understanding to demonstration scale. Properties improvement: - increasing reaction enthalpy/energy storage capacity, - tuning desorption temperature, - improving hydrothermal stability, - tailoring water sorption properties
	Salt hydrates in porous matrix Polymers based encapsulation salt hydrates [37-43]	Combining Absorption, Chemical reaction & Adsorption	 Combining active materials  Functionalization	Design of smart TCM composites -Higher reaction enthalpies; -Water adsorption capacity/storage improvement -Tailoring hydrophilicity -Mass and heat transfer enhancement -Thermal conductivity enhancement

Thermal energy storage at temperatures in the range of 30 to 140 °C is of great interest in the building sector, as well as in industry. This stored energy can be used for space or domestic hot water heating, as the heat input in Organic Rankine Cycle (ORC) or used directly in most industries, e.g., for steam generation. However, a storage solution that fully meets requirements such as compactness, cost, versatility and power is still lacking for this temperature range. Following these concepts, the aim of this article is to present two examples focused on materials optimization for thermal energy storage using PCMs (solid-solid phase transitions) and TCMs (combined sorption and chemical reactions). We show that optimization of these materials leads to enhancing energy storage density, tuning the working temperatures (PCM) and increasing durability of the TCM composites by choosing gamma-alumina as the proper matrix. Moreover, the choice of the matrix is an important task in the production of TCM composites. Crystalline γ-alumina was chosen due to its high density and thermal conductivity (30 W/m·K), which can further promote heat transfer in the system. The γ-alumina matrix with mesopores of 5 nm provided a stable nano-environment for the salts inclusion, which exhibited high energy storage densities and excellent cycling stability of the γ-alumina-$CaCl_2$ composite under working conditions for space heating. Furthermore, for the silica-PEG-salt composites, an original strategy is described which consists of producing the composite material directly and very simply on the basis of the salt, the polymer (PEG) and the silica. Due to its complexing properties towards the salt, the PEG polymer enables a very stable incorporation of the salt into the composite material.

Tailor-made PCMs. The most commercially viable TES technologies currently rely on solid materials, particularly those utilizing the sensible heat of substances like rocks, sand, bricks or concrete. These materials are cost-effective, and their solid state simplifies the TES system by potentially eliminating the need for a heat exchanger allowing for direct contact between the heat transfer fluid and the thermal storage material. However, there is significant potential to explore solid-solid phase change materials, combining the compactness of PCMs with the simplicity and low cost of solid materials. One promising category of solid-solid PCMs is organic plastic crystals (OPCs). These molecules undergo reversible solid phase transitions from a low-temperature ordered structure (tetragonal, orthorhombic, monoclinic, etc.) to a high-temperature orientationally disordered phase (face-centered or body-centered cubic) known as the plastic phase. The polyalcohol series of these materials include pentaerythritol (PE), pentaglycerine (PG) and neopentylglycol (NPG). The solid phase transition in these plastic crystals occurs at temperatures between 44 °C (NPG) and 185 °C (PE). It is characterized by an unusually high enthalpy of transition, ranging from 110 $J.g^{-1}$ (NPG) to 300 $J.g^{-1}$ (PE). OPCs have garnered significant attention for their potential in improving energy storage capacity and versatility [45-47]. In terms of versatility, these materials can be combined in binary and ternary systems to linearly modify the transition temperatures, allowing for a broad range of applications covering temperatures from 20 °C to 250 °C. The NPG:PG combination can cover transition temperatures from 40 °C to 80 °C. To bridge the temperature gap between 80 °C and 190 °C, the PE:PG system can be used [48]. To enhance their energy storage capacity, a new class of shape-stabilized phase change materials (SSPCMs) was proposed [45]. These SSPCMs combine a polyalcohol with adjustable solid phase transition (NPG/PG or PE/PG mixture) with a cheaper and higher latent heat solid-liquid PCM (paraffin wax). The SSPCMs have shown enhanced volumetric latent heat storage capacity (up to 45% compared to pure polyalcohols) without any detrimental effect on discharging power. This combination is interesting for phase change temperatures below 100 °C, since above that temperature the high latent heat of the OPCs

makes them interesting on their own. Although extensive research has been conducted on OPCs and their phase diagrams [49-55], the synthesis and optimization processes for binary systems remain underexplored in the literature. A significant gap exists in the detailed evaluation of their thermal properties and the refinement of protocols that can fine-tune these materials for specific industrial applications. This work presents a detailed approach to obtain a PE:PG system tailored for thermal energy discharge at 140 ºC. The challenges of optimizing thermal behavior through a carefully designed processing protocol are specifically addressed. By systematically adjusting the synthesis parameters, we achieve a material that not only meets the thermal discharge requirements for critical processes like steam production but also demonstrates optimized storage capacity. The targeted discharge temperature is particularly critical for steam production processes, which are widely used across various industries such as food and beverage, chemical, and paper manufacturing. Ensuring a consistent discharge temperature and pressure is crucial for optimizing efficiency and ensuring the reliability of these processes. Moreover, current PCM options within this temperature range face significant stability challenges. For instance, sugar alcohols suffer from excessive supercooling due to polymorphism, while fatty acids are prone to oxidation and degradation. The development of stable and efficient PCMs that can reliably operate at 140°C is therefore crucial, as it would address the current limitations and enhance the performance of TES systems, directly benefiting industrial applications that rely on consistent and high-quality steam production.

Tailor-made TCMs. Thermochemical energy storage offers the possibility to achieve high energy storage density compared to sensible and latent heat storage, as well as low thermal loss to the ambient during the storage period [56]. This technology is also known as a thermal battery [57] since it stores heat and is based on the reversible adsorption (exothermic phenomenon) and desorption (endothermic phenomenon) of gaseous adsorbate (water, ammonia, methanol, ethanol) on solids (adsorbents) or liquids (absorbents) and on chemical reaction or a combination of both. A large number of solids are currently considered for thermochemical heat batteries: thermally stable porous solids like zeolites [32, 33] aluminophosphates [34], metal organic frameworks (MOFs) [35] and zeolitic imidazolium frameworks (ZIFs) [36], and inorganic solids like salt hydrates [58], metal oxides [59] and hydrides [60], as well as two or multi-component sorbents or composites of salts (LiCl, $CaCl_2$, $MgSO_4$, $SrCl_2$, SrBr. etc.) integrated into porous matrices (vermiculite, silica gels, ordered mesoporous silicates, various porous carbons, silicon foam, zeolites, metal organic frameworks) [61-65]. The wide variability and chemical adaptability of these materials offer a great opportunity for targeted design of novel adsorbents tailored to specific applications, e.g. space and water heating. The efficiency of the sorption-based TES technology depends on the sorbent effective functioning: such as a i) high sorption capacity, leading to a high energy storage density of the sorbent, ii) adequate desorption temperature and sorption kinetics, iii) durability under hydrothermal conditions and iv) hysteresis-less adsorption-desorption isotherms [42]. The salt-composite sorbents, which consists of a hygroscopic salt confined in a porous matrix, are currently the most studied TCM water sorbents for low-temperature heat storage due to their high heat storage capacities across various operating conditions. The main advantage of these water composite sorbents is the possibility to enhance their performance by tailoring sorption properties. This can be done through i) varying type, amount and particle size of the incorporated salt, ii) modifying structural properties of the porous matrix (pore size/shape, pore volume and chemical composition) and iii) working on matrix-salt interactions [38]. An essential aspect of preparing a salt hydrate composite TCM is the selection of an appropriate porous matrix for the salt inclusion. The

matrix must fulfill several requirements, such as the ability to provide a stable nano-environment for the salt inclusion, hydrothermal stability, preserve the pore structure under operating conditions, be inert to salt hydrates, and possess good thermal conductivity to enhance the performance of the composite. Additionally, the preparation method should be straightforward and environmentally friendly. Three main methods are used to stabilize salt hydrates in matrices: wet impregnation, incipient wetness impregnation and microencapsulation. The design of two-component sorbents with higher thermal conductivity compared to salts or nanoporous silicates led to the selection of a mesoporous γ-alumina matrix with the average pore sizes of 9.1 and 11.3 nm, prepared by solvothermal and hydrothermal synthesis, respectively, in order to design thermochemical composite water sorbents with $CaCl_2$ and LiCl [42].

Finally, an original strategy is described which consists of directly and very simply producing a composite material based on salt, a polymer (PEG) and silica. The PEG polymer, because of its complexing properties towards the salt, enables the salt to be very stably integrated into the composite.

1.2 Materials and methods

Tailor-made PCMs: The PE:PG system is composed of 1,1,1-tris(hydroxymethyl)ethane (Pentaglycerine) and 2,2-bis(hydroxymethyl)-1,3-propanediol (Pentaerythritol), both supplied by Sigma-Aldrich and used as solid-solid PCM. To evaluate the processing of the binary system, the as-received powders of PE and PG were mixed in a mortar at the proportions specified in Table 3. After an initial manual homogenization, the PE:PG mixture was milled using an 8000 M Mixer/Mill® High-Energy Ball Mill, from SPEX SamplePrep LLC. The milling was performed with two 8 g metallic balls for 4 g of the binary mixture over a period of 30 min. Subsequently, the powder is subjected to different thermal treatments detailed in the next section. The evaluation of the processing was conducted on the PE:PG binary system with a pentaerythritol molar fraction (X_{PE}) of 0.5. After establishing the synthesis procedure, the target discharge temperature was analysed and determined by varying the PE mole fraction in the PE:PG system between 0.69 and 0.85. The following table presents the mass fraction of each component used for the corresponding evaluated composition.

Table 3. Mass fractions of PE and PG for each corresponding PE molar fraction.

X_{PE} (molar fraction)	PE mass (mg)	PG mass (mg)
0.5	0.53	0.47
0.69	0.72	0.28
0.71	0.74	0.26
0.73	0.75	0.25
0.75	0.77	0.23
0.77	0.79	0.21
0.79	0.81	0.19
0.81	0.83	0.17

0.83	0.85	0.15
0.85	0.87	0.13

Differential Scanning Calorimetry (DSC Q2500, TA Instruments, using sealed aluminum crucibles) was used to evaluate the thermal properties of the PE:PG system (latent heat and transition temperatures). Heating/cooling cycles at 5 ºC.min^{-1} up to different maximum temperatures were carried out. The mass of the samples was ca. 9 mg. Argon (50 ml.min^{-1}) was employed as purge gas. The accuracy in the determination of transition temperatures and enthalpies are ± 0.5 °C and ± 5%, respectively. The transient hot disk method was used to measure the thermal conductivity of the sample at room temperature. The measurements were carried out on cylindrical-shaped samples (diameter: 22 mm, thickness: 5 mm). A TPS 2500 S instrument equipped with a Kapton sensor of 2.001 mm in diameter (sensor type 7577) was employed for measurements. The power applied to the rear face of the sample was 20 mW during 20 s. The true density of the polyalcohol binary mixture was determined by helium pycnometer Micromeritics Accupyc 1340 at room temperature. TGA determined the thermal stability of the compounds in a Netzsch ASCII instrument. The sample (10 to 20 mg) was placed in an open alumina crucible under N_2 atmosphere (60 ml.min^{-1}) and heated from 130 ºC to 200 °C in 10 ºC steps, keeping an isotherm temperature for 15 minutes in each step.

Tailor-made TCMs: The commercial granulated γ-alumina, provided by Silkem company (Slovenia), served as the matrix for functionalisation with various hygroscopic salts ($CaCl_2$, LiCl and $MgCl_2$). Composites were prepared applying incipient wetness impregnation method. LiCl, $MgCl_2$ and $CaCl_2$ were dissolved in 1 mL of distillated water, respectively. 1 g of γ-alumina was dried at 120 °C for 2 hours before the incipient wetness impregnation with the prepared solutions, which was performed at room temperature. The obtained composites were dried overnight at room temperature.

The X-ray powder diffraction (XRPD) patterns were recorded on a PANalytical X'Pert PRO high-resolution diffractometer (Almelo, The Netherlands) with Alpha1 configuration using $CuK_{\alpha 1}$ radiation (1.5406 Å) in the range from 10 to 60° 2θ with a step of 0.034° per 100 s using a fully opened X'Celerator detector. Nitrogen physisorption measurements were performed at 77K on a Tristar3020 volumetric adsorption analyzer (Micromeritics, Norcross, GA, USA). Before the adsorption analysis, the samples were outgassed under vacuum for 1 hour at 90 °C and 2 hours at 110 °C in the port of the adsorption analyzer. Prior to the evaluation of textural properties of the composites, the amount of the nonporous salt, which does not contribute to nitrogen adsorption to a large extent, was taken into account. Thus, nitrogen isotherms, specific surface areas and pore volumes were corrected [38]. The BET specific surface area was calculated from adsorption data in the relative pressure range from 0.05 to 0.2. The total pore volume was estimated based on the amount adsorbed at a relative pressure of 0.98. The maximum of the PSD curve was considered as the pore diameter. Elemental analysis was performed by energy dispersive X-ray analysis (EDAX) with an INCA Energy system attached to a Zeiss SupraTM 3VP microscope (Jena, Germany) and by ICP-OES using sprectrometer ES 715 (Varian).Desorption temperatures of the composites were determined by the thermogravimetric analyzer Q5000IR (TA Instruments, USA). For all measurements, samples were heated in air with a heating rate of 10 °C/min. Prior to the TG measurements, samples were stored in a desiccator over saturated potassium sulfate solution for 5 days. The temperature of the maximum (Tpeak) was considered as the desorption temperature. Water adsorption isotherms were measured by gravimetric analyzer IGA -100 (Hiden Isochema Ltd., Warrington, UK) at 25 °C by setting equal pressure intervals of 1.6

mbar between vacuum and 40 mbar with an equilibrium time of 80 s. Before adsorption measurements, the samples were outgassed to a constant weight under ultrahigh vacuum (< 10^{-5} mbar) at 120 °C for 4 hours. The integral enthalpy of adsorption Q_{ads} can be calculated by the following equation: $Q_{ads} = \Delta H_{ads} (w_{ads} - w_{des})$ [kJ/kg_{ads}], where Q_{ads} [kJ/kg_{ads}] is the enthalpy of adsorption, which can be considered as the achievable heat storage density at a material level; ΔH_{ads} [kJ/kg_{water}] is the differential enthalpy of adsorption referred to the adsorbed amount of water; w_{ads} and w_{des} [kg_{water}/kg_{ads}] are the maximum and minimum adsorption amount of water over the adsorbent material at the given boundary conditions. The value of the differential enthalpy of sorption was calculated through the measurement of the equilibrium water sorption curves (at 298 K and 308 K) according to the Clausius-Clapeyron equation. The sorption/desorption cycling performance or hydrothermal stability was determined on IGAsorp-XT automated water sorption analyzer (Hiden Isochema Ltd., Warrington, UK.) with the sequential procedure of water uptake measurements at 40 °C under moist nitrogen gas flow (flow rate of 250 mL/min and 80% relative humidity) for 3 h, followed by drying at 100 °C with dry nitrogen flow for 2 h. The water vapor pressure during desorption and adsorption of the samples was set to 12.5 mbar (a dew point temperature of 10 °C). The difference of adsorbed water amount at 40 °C and 100 °C at 12.5 mbar is the cycle (water) loading lift of the composite.

The silica-PEG-salt composites were prepared with the sol-gel method using the following compounds: tetraethoxysilane ($Si(OEt)_4$) (Aldrich 98%), polyethylene glycol 600 (Merck), HCl (37 wt.%) and calcium chloride dihydrate $CaCl_2 \cdot 2H_2O$ or magnesium chloride hexahydrate $MgCl_2 \cdot 6H_2O$ (Aldrich 99%). The first step is the dissolution of the chosen salt hydrate (3.2 g) and of PEG-600 (2 g) in an HCl aqueous solution at 3.7 wt.% (14 g). Tetraethoxysilane (8 g) is then added to the mixture with agitation during two hours. Next, the obtained colloidal suspension is heated to 50 °C for 24 h and progressively turns into a gel. The latter is finally dried at 60 °C during 24 h and then at 100 °C during 24 h, and broken into millimetric fragments. For comparison purposes, a salt-free control sample was also prepared. Table 4 summarizes the theoretical composition of the two composites. Sample 1 contains 36 wt.% of calcium chloride, associated to silica and PEG as the matrix. Sample 2 contains 25 wt.% of $MgCl_2$. The salt contents are close to those reported in previous studies about silica gel / $CaCl_2$ and silica gel / $MgCl_2$ composites for heat storage or cooling applications [64-66].

All tailor-made TCM composites are listed in Table 4.

Table 4. Theoretical weight composition of the synthetized composite TCM samples

	incorporated salt	anhydrous salt content (wt.%)	SiO_2 content (wt.%)	PEG content (wt.%)
Sample 1	$CaCl_2$	36	34	30
Sample 2	$MgCl_2$	25	40	35
γ-alumina-10 LiCl	LiCl	10	-	-
γ-alumina-10 $CaCl_2$	$CaCl_2$	10	-	-
γ-alumina-7 $MgCl_2$	$MgCl_2$	7	-	-

1.3 Tailor-made PCMs: Results

1.3.1 System processing and transition temperature adjustment

The PE:PG system is widely reported in the literature, however, the processing required to obtain it is omitted. Although the whole system is generally melted and then solidified, this process is not the most optimal from an economic point of view due to the energy required for the casting process, nor for the final properties obtained in the system. To evaluate the effect of heat treatment on the formation of the binary system, a PE:PG sample, after a grinding process, has been subjected to thermal cycles up to different maximum temperatures, reaching the melting of the system in the final cycles, simulating a casting process. This evaluation has been carried out on a stoichiometric binary system (X_{PE}=0.5), hereinafter defined as $PE_{0.5}$:PG.

Figure 1a gathers the thermograms obtained during different thermal cycles, indicating the onset temperature and enthalpy of the phase transition, both observed during the cooling stage. The first two thermal cycles (bottom) cover a temperature range up to 160 °C, encompassing the theoretical solid-solid transition temperature of the system (X_{PE}=0.5). Subsequent cycles extend up to the solid-solid transition temperature of PE, reaching 190 °C and 210 ºC. Finally, a temperature of 260 °C is achieved, reaching the theoretical liquidus line of the system [45] (consistent with findings from previous studies) and causing melting of the compound. As observed in the thermogram, the maximum latent heat attained in the system (indicating system formation) is obtained after thermal cycling and reaching the solid-solid transition of PE (190 ºC). The $PE_{0.5}$:PG transition occurs at 120 °C with an enthalpy of 177 $J \cdot g^{-1}$. Another signal of the system's formation is the disappearance of the PG solid-solid transition peak (89 ºC), which is minimum after the thermal cycling up to 190 ºC. It is worth noting that if we reach the melting point of the plastic crystal, the conditions of solidification (solidification rate) can significantly impact the final thermal properties, potentially leading to a decrease in latent heat and signs of phase segregation. This phenomenon is observable in the last two cycles conducted in the DSC, where, upon melting the material at 225 °C, the energy release cycle exhibits a reduction in latent heat by up to 40.5 $J.g^{-1}$ in the solid-solid transition. Therefore, it is only necessary to perform a milling process, followed by thermal cycling around the solid-solid transition of the system (covering the transition temperature of PE) to synthesize the binary system. It should be noted that, although the synthesis procedure for the described binary system has achieved optimal thermal properties, minimizing the phase transition detected at 89 °C, this signal has not completely disappeared. This could indicate a certain demixing in the system, potentially affecting its stability during cycling. This point requires further investigation, including an evaluation of the stability during cycling as well as at different heating/cooling rates.

Once the procedure for obtaining the binary system has been established, we can adjust the system for a discharge temperature of 140 °C. In Figure 1b, we can observe that the system with X_{PE}=0.69 (hereinafter $PE_{0.69}$:PG) exhibits a discharge transition temperature of 140 °C (at a cooling rate of 5 $°C.min^{-1}$). It is also interesting to note that the subcooling of the system decreases from 10 °C for X_{PE}=0.85 to 5 °C for the X_{PE}=0.69 system. This reduction makes this material a more interesting compound for its application in TES systems.

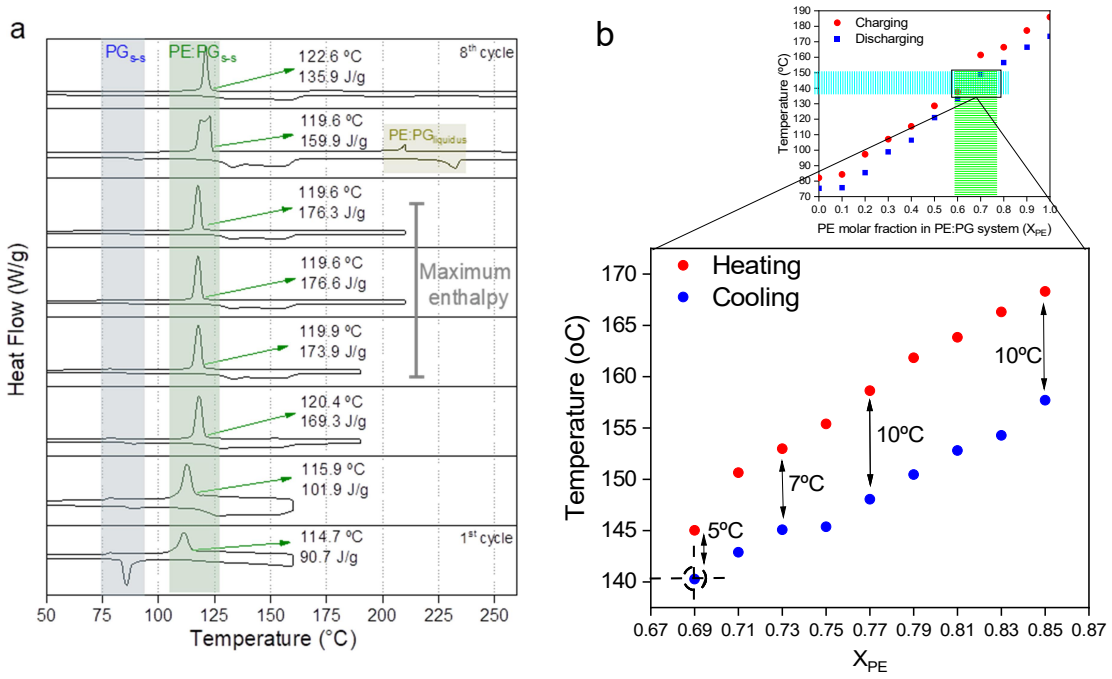


Figure 1. a) Thermograms of $PE_{0.5}$:PG during the thermal cycling, and b) tailoring the discharging transition temperature of the binary system.

1.3.2 Main thermal properties

Considering TES applications, the main thermal properties of the tailored $PE_{0.69}$:PG system have been determined. Table 5 includes its latent heat, true density, volumetric latent heat, thermal conductivity, and the specific heat capacity in crystal and plastic phases.

Table 5. Main thermophysical properties of PE:PG (X_{PE}=0.69).

ΔH ($J \cdot g^{-1}$)	ρ ($g.cm^{-3}$)	ΔH ($MJ \cdot m^{-3}$)	$k_{crystal\ phase}$ ($W \cdot m^{-1} \cdot K^{-1}$)	$Cp_{crystal\ phase}$ ($J.g^{-1} \cdot K^{-1}$)	$Cp_{plastic\ phase}$ ($J.g^{-1} \cdot K^{-1}$)
188.2	1.33	250.0	0.59	≈2.2	≈2.8

To explore the real potential of these materials, their volumetric heat capacity (considering only the latent heat), specific heat capacity, and thermal conductivity are compared in Figure 2 to other commercially available PCMs (organic PCMs and commercial molten salts) in a similar working temperature range (commercial PCMs data obtained from PCM Products Ltd -pcmproducts.net). The comparison also includes other solid-solid PCMs extensively reported in the literature, namely the dialkyl ammonium salts [67].

In Figure 2a, the specific heat of $PE_{0.69}$:PG is presented for both the crystalline phase (at room temperature) and the plastic phase (above its transition temperature). It can be seen that, in the crystalline phase, the system exhibits a specific heat comparable to other organic PCMs, surpassing the values reported for molten salts and solid-solid dialkylammonium

PCMs. Furthermore, the specific heat in the plastic phase exceeds these values, reaching up to 2.8 $J \cdot g^{-1} \cdot K^{-1}$, highlighting its enhanced thermal capacity in this phase.

In Figure 2b, the volumetric latent heat is shown for the PE:PG system developed in this work, as well as the range of values that can be obtained by positioning the corresponding values of pure PG and PE. The volumetric latent heat of the system is at the upper range of reported values for commercial PCMs at this temperature, making it the PCM with the highest volumetric latent heat around 140 °C. Throughout the temperature range of 80 to 190 °C, it is only surpassed by the solid-liquid PCMs H120 and A164, which would require macro/microencapsulation or confinement through a heat exchanger, significantly reducing the overall energy density of the system.

Lastly, Figure 2c shows the thermal conductivity of the $PE_{0.69}$:PG. These materials exhibits considerably higher thermal conductivity than their dialkylammonium counterparts and organic PCMs, being slightly higher than the values reported for molten salts. This high conductivity makes them particularly attractive for applications requiring high energy charging and discharging rates, which can be further enhanced by doping with conductive particles (e.g., expanded graphite). Since these materials maintain their solid state, no segregation or agglomeration of the dopant particles is expected during thermal cycling.

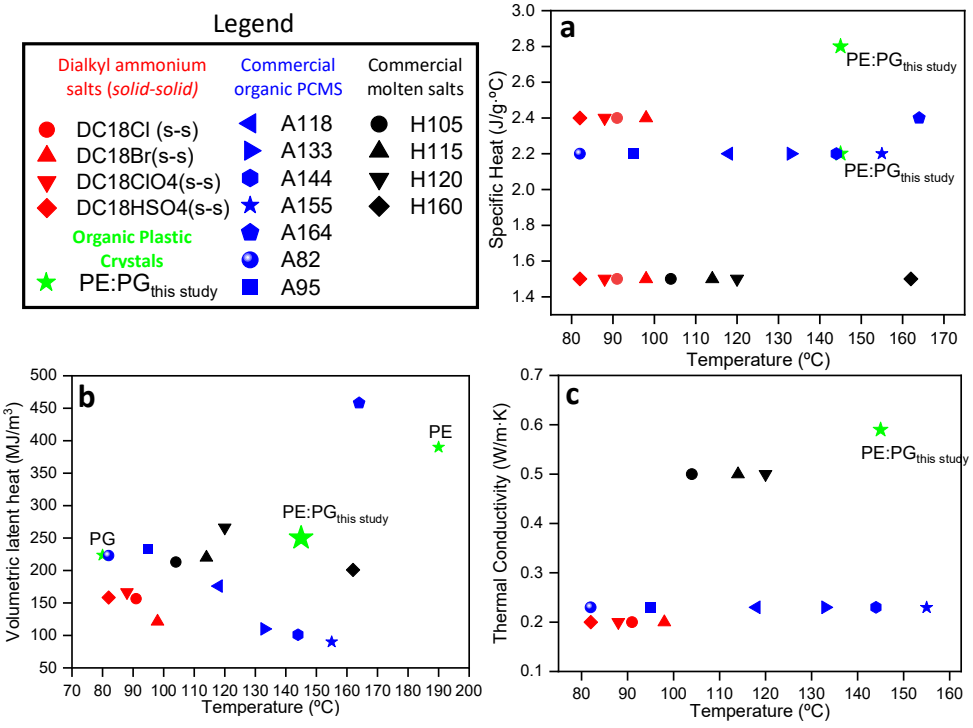


Figure 2. Comparison of a) specific heat, b) volumetric latent heat, and c) thermal conductivity of $PE_{0.69}$:PG with other commercially available PCMs (PCM Products Ltd) and reported solid-solid PCMs based on dialkyl ammonium salts [67] .

1.3.3 Thermal stability evaluation

To assess the thermal stability of $PE_{0.69}$:PG, a thermogravimetric analysis was conducted on the material. Figure 3a illustrates the mass loss observed during heating, displaying two distinct slopes in the mass-time curve. According to the literature [68], the mass loss experienced by pure plastic crystals in their plastic phase corresponds to a

sublimation process. To gain deeper insights into this phenomenon, we employed the calculation method proposed by R. Barron [69]. By utilizing the Clausius-Clapeyron equation and the Langmuir equation (Eq. 1), the sublimation temperatures (T_{sub}) for each slope were determined by intersecting the ordinate axis on the graph $log(m_{sub} \cdot T^{1/2})$ vs $1/T$ (Figure 3, right). Here, ΔH_{sub} represents the enthalpy of sublimation, M_w denotes the molar mass, and m_{sub} indicates the slope of mass loss with respect to temperature for each isotherm.

$$log(m_{sub} \cdot \sqrt{T}) = \frac{-0{,}0522(\Delta H_{sub})}{T} + \left[\frac{0{,}0522(\Delta H_{sub})}{T_{sub}} - \frac{1}{2} log\left(\frac{1306}{M_w}\right)\right] \quad (1)$$

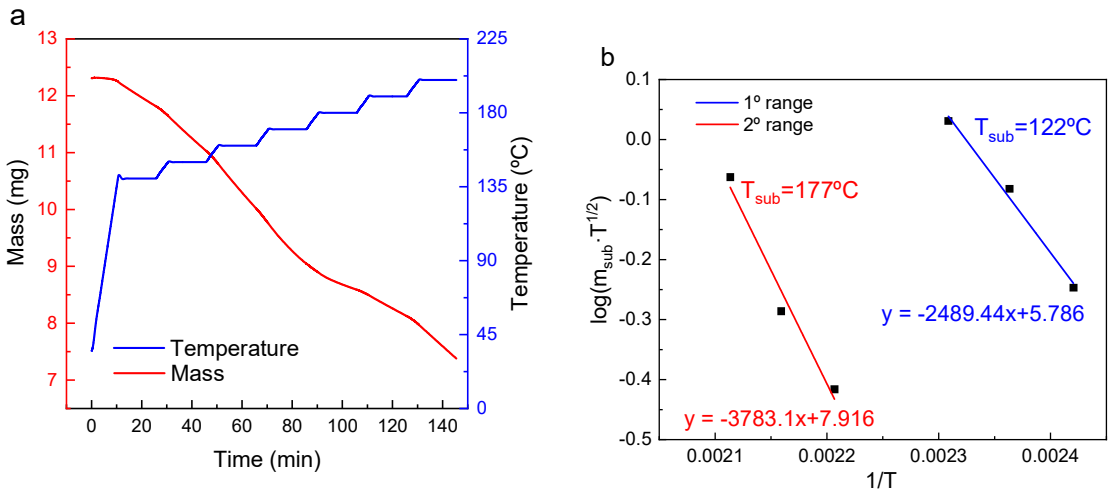


Figure 3. TGA of a) $PE_{0.69}$:PG and b) $log(m_{sub} \cdot T^{1/2})$ vs 1/T to obtain the sublimation temperatures.

The sublimation temperature for each segment indicates the point at which each component of the system begins to sublime, measuring 122 °C and 177 °C, with the latter corresponding to the contribution of PE. Both temperatures, close to the solid-state transition temperature of the material, lead to material loss through sublimation during heating under atmospheric pressure conditions. Considering that these temperatures are in the operating range of the system, the need to develop a coating or container that prevents the loss of material under these conditions becomes manifest.

1.4 Tailor-made TCMs: Results

1.4.1. Structural properties

The composites were analysed by X-ray powder diffraction to determine structural properties. XRD patterns of the prepared composites and salt hydrates taken from the XRD database are shown in Figure 4. It can be observed that γ-alumina in the composites did not change its crystal structure during incipient wettness impregnation. The diffraction peaks of γ-Al_2O_3 are rather broad, which can be due to nanosized particles. No additional diffraction peaks of the salts are observed in the XRD patterns indicating that all salts were successfully confined within the mesopores of the matrix (with an average pore size of 5.1 nm). The amount of the incorporated salts slightly differ in the composites: 10 wt.% of LiCl, 10 wt.% of $CaCl_2$ and 7 wt.% of $MgCl_2$.

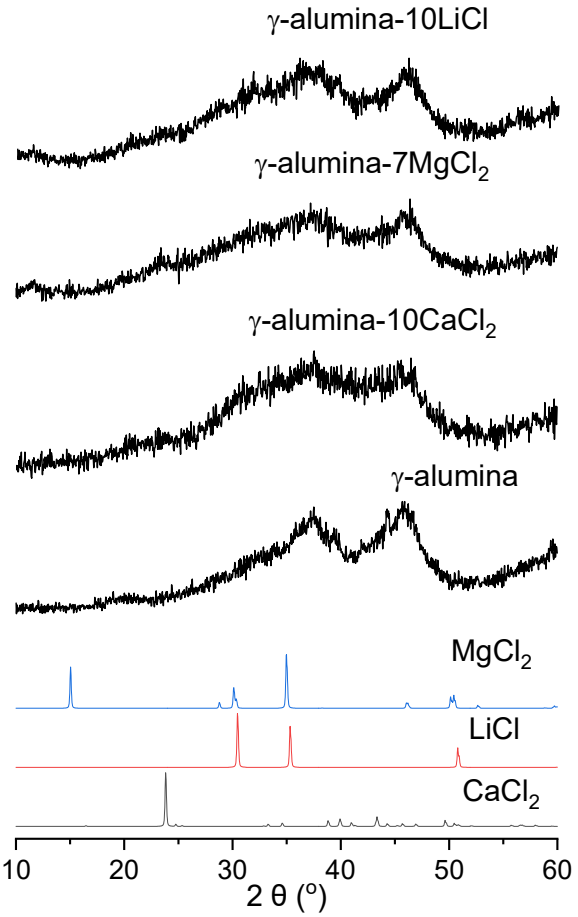


Figure 4: PXRD of γ-alumina, composites and salt hydrates ($CaCl_2$, LiCl, $MgCl_2$)

Desorption temperature for the composites were determined using thermogravimetry. The DTG curves (Figure 5) show the total water loss at different temperatures for both the hydrated composites and the matrix. For instance, the $CaCl_2$ composite requires the highest temperature of 170 °C to remove all the water. The total water loss determined at 170 °C was 16.6% for the matrix, 33.9% for the $CaCl_2$ composite, 23.6% for the $MgCl_2$ composite and 24.0% for the LiCl composite. The desorption temperatures of the composites are higher than that of the matrix (120 °C), showing that salts are effectively confined within the matrix.

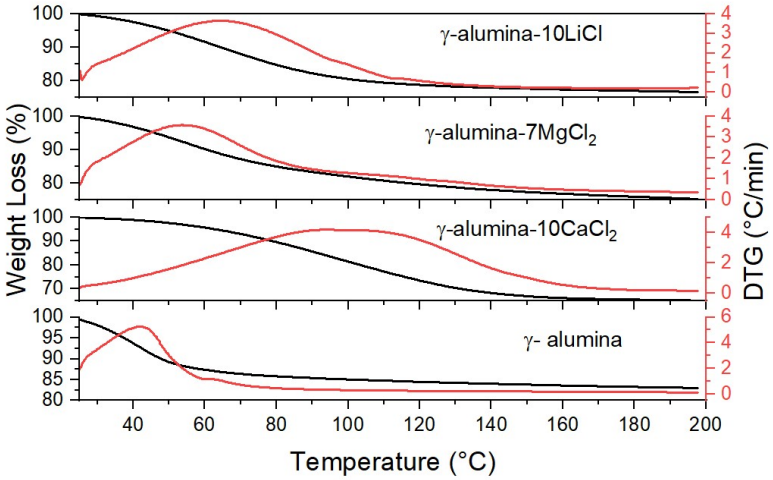


Figure 5: TG-DTG curves of the composites and γ-alumina

Nitrogen physisorption measurements were used to elucidate textural properties of γ-Al_2O_3 and its composites (Table 6). Salt incorporation in the matrix decreases specific surface areas, pore volumes and pore sizes.

Table 6. Textural properties, water loading lift and the integral heat of adsorption

Sample	S_{BET} ($m^2 \cdot g^{-1}$)	Vpore ($cm^3 \cdot g^{-1}$)	Pore size (nm)	Δw ($kg \cdot kg^{-1}$)	Q_{ads} ($kWh \cdot m^{-3}$)
γ-alumina	220	0.403	5.1	0.063	174
$10CaCl_2$	108	0.261	4.2	0.254	700
10LiCl	136	0.230	4.5	0.257	711
$7MgCl_2$	83	0.149	4.3	0.120	334

1.4.2 Sorption and heat storage properties

The composites were monitored by water sorption isotherms at 25 °C to determine their maximal water sorption capacity and sorption kinetics. Figure 6 presents water sorption isotherms, indicating different hydrophilic behaviour of the composites. The maximum water uptake for the different composites was as follow: LiCl (80.3%), $MgCl_2$ (67.8%) and $CaCl_2$ (66.5%). However, at a relative pressure p/p_0 of 0.4, the order changes to : $CaCl_2$ (44.7%), LiCl (31.9%) and $MgCl_2$ (29.1%). Comparing the water sorption isotherms within the range $0 < p/p_0 < 0.2$, shows that the LiCl sample exhibits higher water uptake than the $CaCl_2$ and $MgCl_2$ composites. At a relative pressure of 0.4, the $CaCl_2$ composite with an average mesopore size of 4.2 nm and a total pore volume of 0.261 $cm^3 \cdot g^{-1}$ has a water that is 15.5% higher than that of the $MgCl_2$ composite which has a slightly larger mesopore diameter (4.3

nm) and smaller total pore volume (0.120 $cm^3.g^{-1}$). This difference is likely due to the lower $MgCl_2$ content in the latter composite.

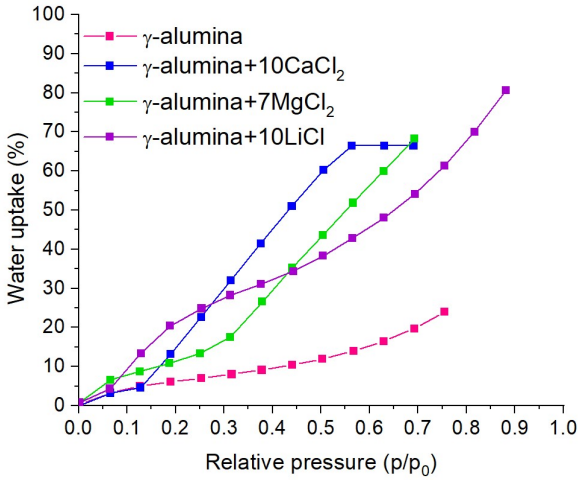
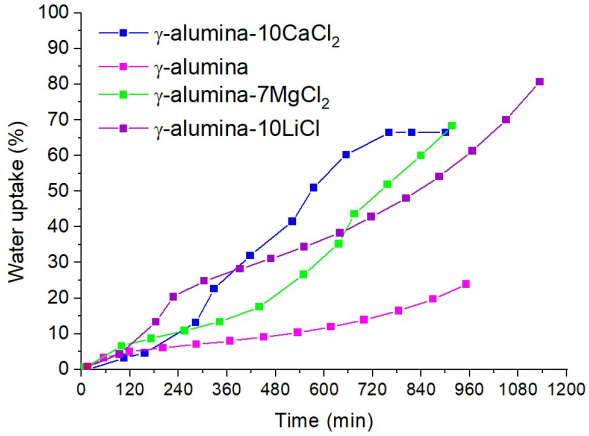


Figure 6: Water sorption isotherms at 25 °C

The kinetic uptake curves are plotted Fig. 7 showing slow sorption kinetics for all the composites. The $CaCl_2$ composite reaches the maximal water uptake in 12.5 hours. In contrast, the LiCl composite requires 19 hours to complete water uptake, which is significantly longer compared to the LiCl composite with the γ-alumina matrix with larger mesopores (9.3 nm), prepared with the bottom up synthesis [42]. This can be explained by the presence of smaller mesopores in the studied composite and stronger salt-matrix interactions. The rate of water sorption increases gradually during the first two hours for all the composites. The $MgCl_2$ and LiCl composites show the highest sorption rate, whereas the $CaCl_2$ composite shows the slowest rate with the lowest water uptake (3.5%). After two hours, sorption has started increasing with higher rates for $CaCl_2$ and LiCl, while a slower rate has been observed for the $MgCl_2$ composite. Water uptake is completed in the following order from $CaCl_2$, $MgCl_2$, to LiCl.

The most relevant parameter for evaluating the effectiveness of a sorbent for TES is the integral heat of adsorption or energy storage density. Table 6 shows water loading lift and the integral heat of adsorption for the composites under working conditions (adsorption temperature of 30 °C at 12.5 mbar water vapor pressure and desorption temperature of 100 °C). The γ-alumina-10LiCl and -10$CaCl_2$ composites exhibit a similar water loading lifts which is approximately two times that of γ-alumina-7$MgCl_2$ composite. Additionally, the water uptakes and energy storage densities of the composites are higher than the composites presented in [42], showing that mesopores up to 5.1 nm are more advantageous for sorption heat storage performance, although the same amount of $CaCl_2$ and LiCl was confined.

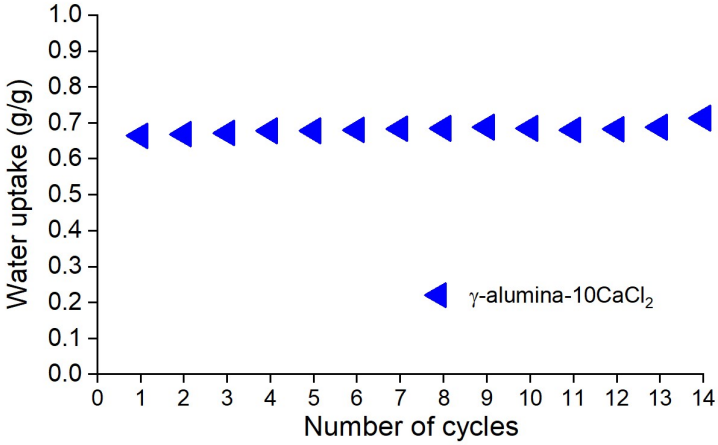


529

530 **Figure 7**: Sorption kinetics at 25° C of γ-alumina and the composites

531 It can be concluded that the composites with a γ-alumina matrix, possessing smaller
532 mesopores, are beneficial for thermal battery use for space heating. Similar energy storage
533 densities of 700 and 711 kWh·m^{-3} have been determined for the $CaCl_2$ and LiCl composites,
534 respectively, while the $MgCl_2$ composite shows lower energy storage density (334 kWh·m^{-3}).

535 The repeated cycling stability, which indicates durability (Figure 8) of the $CaCl_2$
536 composite, was evaluated, demonstrating an excellent initial hydrothermally stability. No
537 decrease in water uptake was observed after 14 cycles between temperatures of 100 °C and
538 40 °C under a water vapor pressure of 12.5 mbar.



539

540 **Figure 8**: Cycling stability of 14 cycles of sorption and desorption for the γ-alumina-
541 10$CaCl_2$ between 100 °C and 40 °C under the water vapor pressure of 12.5 mbar.

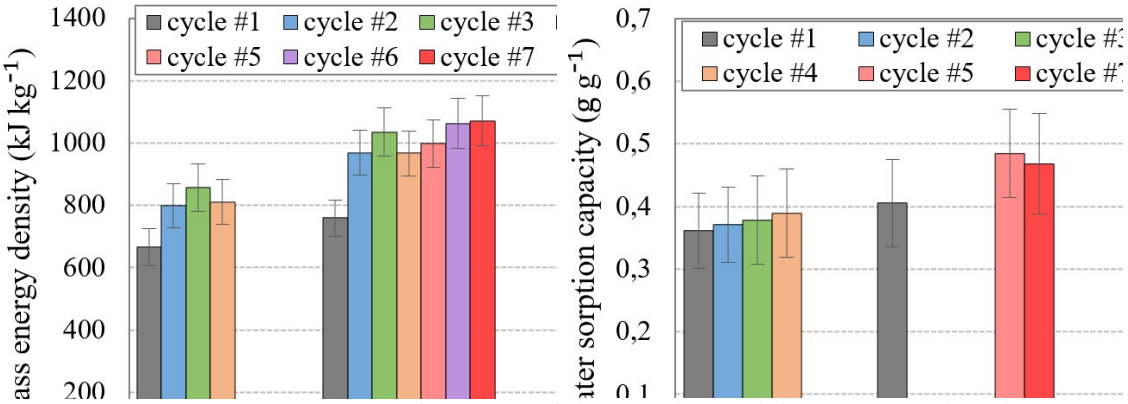
542

543 **1.5 Experimental heat storage setup**

544 The silica-PEG-salt composite TCM was selected for laboratory scale cycling
545 experiments at a more representative scale (above 50 grams). Here, the novelty lies in the use
546 of a new and easy synthesis strategy (one-pot method) to produce the silica-PEG-salt
547 composites. Using this simple method, a significant stabilization of the salt inside the
548 composite material is possible. This is due to the PEG polymer, whose complexing properties

549 towards the salt reduce the risk of deliquescence. A fixed bed insulated reactor with 46 mm
550 inner diameter made of stainless steel was used for this purpose, as described in [61]. The
551 experimental setup includes a heating device and a bubbling humidifier associated to a
552 thermostatic bath to control the temperature and humidity of the air entering in the reactor. A
553 mass flow controller regulates the inlet air flow rate, with an uncertainty of 0.2 NL min^{-1}.
554 During the experiments, the reactor is filled with 56 ± 4 g of TCM and crossed by a
555 constant dry air flow rate of 8.2 ± 0.8 $NL.min^{-1}$. The corresponding bulk velocity is about
556 0.1 $m{\cdot}s^{-1}$. The procedure involves several steps: (1) The dehydration of the material under dry
557 air at 130 °C for four hours. During this charging (or desorption) phase, the humidifier is by-
558 passed. (2) Once the reactor has cooled down to room temperature, moist air is sent into it.
559 The relative humidity for the discharging (sorption) phase was set to 42% (12.1 mbar water
560 vapor pressure) and the temperature at the reactor inlet to 30 °C. (3) The first steps are
561 repeated. Four to seven successive desorption / sorption cycles were realized for each
562 composite TCM.
563 The energy generated by the sorption process and given to the air flow over each cycle
564 can be expressed by mass of dehydrated sample (at 130 °C for four hours). The resulting
565 mass energy densities are presented in Figure 9a. For sample 1 (36 wt.% $CaCl_2$) and sample 2
566 (25 wt.% $MgCl_2$), the obtained value significantly changes between the first and the second
567 cycles, and then stabilizes. The energy density increases by 20% and 28%, respectively, from
568 cycles #1 to #2. This change can be attributed to modifications in the material properties after
569 the first cycle, which enhance water-salt sorption interactions. Figure 9b also shows that the
570 water sorption capacity progressively increases from one cycle to the next. Some values are
571 missing for sample 2 and the control sample because of hygrometer dysfunctions.

572



573 **Figure 9**. Storage performance of the tested materials over several cycles:
574 a) mass energy density, b) water sorption capacity

575 The previous results are averaged in Table 7 for each material over the four to seven
576 completed cycles. Sample 2 exhibits higher energy density and water sorption capacity than
577 sample 1 despite a lower salt content. Its mass (resp. volumetric) energy density is increased
578 by 25% (resp. 40%) compared to sample 1, while its water sorption capacity is 21% greater.
579 The storage properties of magnesium chloride are thus more promising than those of calcium
580 chloride under the studied conditions. Besides, as expected, Table 7 shows that the silica /
581 PEG matrix alone (control sample) contributes negligibly to the energy and water storage.

582

583

Table 7. Average energy densities and sorption capacities of the tested materials (by mass or volume of dehydrated sample)

	sample 1	sample 2	control
energy density ($kJ \cdot kg^{-1}$)	782	980	15
energy density ($kWh \cdot m^{-3}$)	154	216	3
water sorption capacity ($kg_{H2O} \cdot kg^{-1}$)	0.37	0.45	0.02

Considering heat storage applications, the generated power evaluation may be as important as the energy density. Figure 10 enables the comparison of the peak power density of the tested materials for the last sorption cycle. The peak power density of sample 2 (76 $kW.m^{-3}$) is twice that of sample 1 (39 $kW.m^{-3}$). These values are consistent with the temperature curves of Figure 11. Indeed, the outlet air temperature reaches 60 °C for sample 2 and 47 °C for sample 1. Finally, the energy discharged by the control sample barely heats the air flow.

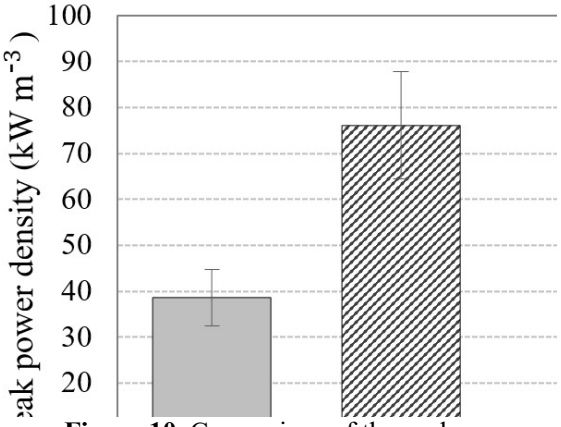


Figure 10. Comparison of the peak power density of the tested materials for the last sorption cycle

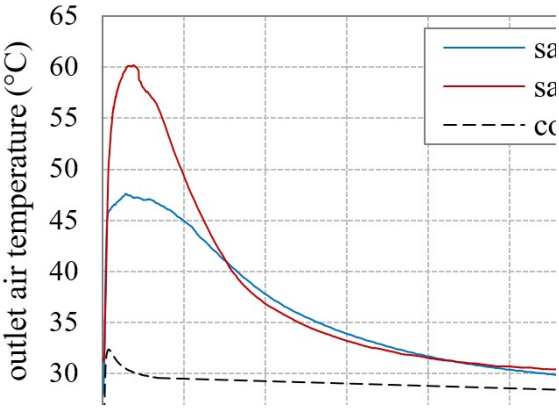


Figure 11. Evolution of the air temperature measured at the outlet of the reactor over the last sorption realized for each material

Conclusions and final remarks.

For tailor made PCMs, the study reveals that the synthesis process of tailored OPCs binary systems, specifically PE:PG, involves a mechanical milling process followed by thermal cycling around the solid-solid transition, eliminating the need for melting the compound during synthesis. The optimized $PE_{0.69}$:PG system achieves a discharge temperature of 140 ºC with a significantly reduced subcooling of less than 4 ºC, making it highly suitable for TES applications in this temperature range. The system exhibits a high latent heat of 177 $J \cdot g^{-1}$, a heat storage density of 250 $MJ \cdot m^{-3}$, and a thermal conductivity of 0.59 $W \cdot m^{-1} \cdot K^{-1}$, outperforming several commercial PCMs between 110 ºC and 170 ºC. This provides a substantial advantage in energy storage capacity, where volumetric latent heat and thermal conductivity are critical parameters. However, the thermal stability analysis highlights the need for protective measures, such as coatings or sealed containers, to prevent material sublimation, which can occur over extended cycles. Additionally, the potential for phase separation and demixing needs to be further evaluated, as this could affect the long-term cycling stability and overall system performance.

For the TCMs, several cycling experiments were conducted under conditions appropriate for space heating applications (i.e., adsorption at 30 °C under a water vapor pressure of about 12.5 mbar, and desorption at 100 °C or 130 °C). For small-scale experiments (about 10 mg samples), the highest maximal water uptake (80.3%) and theorethical heat storage density (711 $kWh.m^{-3}$) were determined for the γ-alumina-10LiCl composite. However, the fastest rate of water adsorption and the best durability under hydrothermal cycling conditions were obtained for the γ-alumina-10$CaCl_2$ composite. The water sorption capacity of the latter reaches its maximum (66.5%) after 12.5 hours and no decrease of water uptake was observed after 14 cycles. The properties of the mesoporous γ-alumina matrix such as high density, particular mesostructure and structural stability are thus advantageous for the production and for the use of these TCM composites for low temperature heat storage. Following the previous small-scale experiments, composites made of a silica-PEG matrix and either calcium chloride or magnesium chloride were characterized in a lab-scale reactor (50 g samples). Under the considered operating conditions, the silica-PEG matrix succeeded in stabilizing hydrated $MgCl_2$ and $CaCl_2$ when the theoretical salt content was 25 and 36 wt.%, respectively. The sample containing 25 wt.% of $MgCl_2$ performed best: its average energy density over seven sorption cycles is 980 $kJ.kg^{-1}$ of dehydrated material (216 $kWh.m^{-3}$) and its peak power density amounts to 76 $kW.m^{-3}$. The composite TCMs exhibited promising heat storage performance. Still, their stability should be properly assessed under a range of operating conditions before scale up and integration in a real application.

Finally, different TES applications may require the use of tailored materials whose optimization is strictly linked to the application requirements. It is possible to optimize various physicochemical properties in order to enhance heat and mass transfer and increase durability. The exploration of multiple optimization routes will be crucial as long as a sufficient number of TES solutions meeting the needs of each application are not available. The examples and results presented in this article highlight the complexity of studying TES materials, while also demonstrating how targeted improvement strategies can fine tune the material properties for potential use in TES applications. Another critical aspect is testing the durability of these materials before scaling up and integrating them into practical systems, to ensure their stability over multiple charging and discharging cycles.

Acknowledgements: This research was funded by The Basque Government (Elkartek CICe2023). The authors also gratefully acknowledge Yagmur Polat and Cristina Luengo for their technical support. The Slovenian Research and Innovation Agency is thanked for the support of the research program P1-0021 (Nanoporous materials). This work was also supported by the French National Research Agency (ANR) in the frame of the STOCK-CAR project (ANR-18-CE05-0044).

References

[1] Salpakari, Jyri; Mikkola, Jani; Lund, Peter D. Improved flexibility with large-scale variable renewable power in cities through optimal demand side management and power-to-heat conversion. Energy Conversion and Management, 2016, vol. 126, p. 649-661. https://doi.org/10.1016/j.enconman.2016.08.041

[2] Airò Farulla, G., Cellura, M., Guarino, F., & Ferraro, M. (2020). A review of thermochemical energy storage systems for power grid support. Applied Sciences, 10(9), 3142. https://doi.org/10.3390/app10093142

[3] Bloess, A., & Schill, W. (2018). P., Zerrahn, A. Power-to-heat for renewable energy integration: A review of technologies, modeling approaches, and flexibility potentials. https://doi.org/10.1016/j.apenergy.2017.12.073

[4] IRENA (2019), Innovation landscape brief: Renewable Power-to-Hydrogen, International Renewable Energy Agency, Abu Dhabi.. https://www.irena.org/-/media/Files/IRENA/Agency/Publication/2019/Sep/IRENA_Power-to-Hydrogen_Innovation_2019.pdf?la=en&hash=C166B06F4B4D95AA05C67DAB4DE8E2934C79858D

[5] Palys, M. J., & Daoutidis, P. (2022). Power-to-X: A review and perspective. Computers & Chemical Engineering, 107948. https://doi.org/10.1016/j.compchemeng.2022.107948

[6] Mitali, J., Dhinakaran, S., & Mohamad, A. A. (2022). Energy storage systems: A review. Energy Storage and Saving. https://doi.org/10.1016/j.enss.2022.07.002

[7] Cabeza, L. F. (2021). Advances in thermal energy storage systems: Methods and applications. In Advances in Thermal Energy Storage Systems (pp. 37-54). Woodhead Publishing. https://doi.org/10.1016/C2013-0-16453-7

[8] Gunasekara, S. N., Barreneche, C., Inés Fernández, A., Calderón, A., Ravotti, R., Ristić, A., ... & Stamatiou, A. (2021). Thermal energy storage materials (TESMs)—what does it take to make them fly?. Crystals, 11(11), 1276. https://doi.org/10.3390/cryst11111276

[9] Borri, E., Zsembinszki, G., & Cabeza, L. F. (2021). Recent developments of thermal energy storage applications in the built environment: A bibliometric analysis and systematic review. Applied Thermal Engineering, 189, 116666. https://doi.org/10.1016/j.applthermaleng.2021.116666

[10] Cabeza, L. F., & Palomba, V. (2022). The role of thermal energy storage in the energy Energy System, 338-350 https://doi.org/10.1016/B978-0-12-819723-3.00017-2

[11] Chavan, S., Rudrapati, R., & Manickam, S. (2022). A comprehensive review on current advances of thermal energy storage and its applications. Alexandria Engineering Journal, 61(7), 5455-5463. https://doi.org/10.1016/j.aej.2021.11.003

[12] Palomba, V., & Frazzica, A. (2019). Comparative analysis of thermal energy storage technologies through the definition of suitable key performance indicators. Energy and Buildings, 185, 88-102. https://doi.org/10.1016/j.enbuild.2018.12.019

[13] Bauer, T., Steinmann, W. D., Laing, D., & Tamme, R. (2012). Thermal energy storage materials and systems. Annual Review of Heat Transfer, 15. https://doi.org/10.1615/AnnualRevHeatTransfer.2012004651

[14] Gil, A., Medrano, M., Martorell, I., Lázaro, A., Dolado, P., Zalba, B., & Cabeza, L. F. (2010). State of the art on high temperature thermal energy storage for power generation. Part 1—Concepts, materials and modellization. Renewable and sustainable energy reviews, 14(1), 31-55.
https://doi.org/10.1016/j.rser.2009.07.035

[15] Tatsidjodoung, P., Le Pierrès, N., & Luo, L. (2013). A review of potential materials for thermal energy storage in building applications. Renewable and Sustainable Energy Reviews, 18, 327-349.
https://doi.org/10.1016/j.rser.2012.10.025

[16] Engel, G., Kerschenbauer, R., Hinteregger, M., Gregorcic, G., Fulterer, A. M., Wagner, W., & Helden, W. V. (2021). Development of a sorption thermal energy storage to support the thermal management of hybrid vehicles. International Journal of Vehicle Design, 85(2-4), 139-153.
https://doi.org/10.1504/IJVD.2021.120411

[17] Tamme, R., Laing, D., Steinmann, W. D., & Bauer, T. (2022). Thermal energy storage. In Solar Thermal Energy (pp. 285-313). New York, NY: Springer US.
https://link.springer.com/referenceworkentry/10.1007/978-1-0716-1422-8_684

[18] Lager, D. (2017). Evaluation of Thermophysical Properties for Thermal Energy Storage Materials—Determining Factors, Prospects and Limitations (Doctoral dissertation, TU Wien). https://doi.org/10.34726/hss.2017.47756

[19] Compact Thermal Energy Storage Materials within Components within Systems https://task67.iea-shc.org/

[20] Rathgeber, C., Schmit, H., Hiebler, S., & Hoock, P. (2021, February). Development of Phase Change Materials Based on Mixtures of Salt Hydrates Through Theoretical Prediction and Experimental Investigation. In 14th International Renewable Energy Storage Conference 2020 (IRES 2020) (pp. 14-18). Atlantis Press.
https://doi.org/10.2991/ahe.k.210202.003

[21] Zhi, M., Fan, R., Yang, X., Meng, Z., Sun, Q., Liu, Q., & He, Y. (2023). Phase diagram prediction and experimental verification of a binary hydrated salt mixture as phase change thermal storage materials. Journal of Energy Storage, 61, 106731.
https://doi.org/10.1016/j.est.2023.106731

[22] Palacios, A., Navarro, M. E., Barreneche, C., & Ding, Y. (2020). Hybrid 3 in 1 thermal energy storage system–Outlook for a novel storage strategy. Applied Energy, 274, 115024.
https://doi.org/10.1016/j.apenergy.2020.115024

[23] Palacios, A., Navarro, M. E., Barreneche, C., & Ding, Y. (2023). Hybridization of Salt Hydrates with Solid–Solid Phase Change Materials: A Novel Pathway to Sorption Thermochemical Materials Manufacturing. Advanced Sustainable Systems, 2200184.
https://doi.org/10.1002/adsu.202200184

[24] Serrano, A., Dauvergne, J. L., Doppiu, S., & Palomo Del Barrio, E. (2019). Neopentyl glycol as active supporting media in shape-stabilized PCMs. Materials, 12(19), 3169..
https://doi.org/10.3390/ma12193169

[25] Ristić, A.; Logar, N.Z.; Henninger, S.K.; Kaučič, V. (2012) The Performance of Small-Pore Microporous Aluminophosphates in Low-Temperature Solar Energy Storage: The Structure-Property Relationship. Advanced Functional Materials, *22*, https://doi.org/10.1002/adfm.201102734

[26] Mal, S., Ristić, A., Golobič, A., Zabukovec Logar, N. (2021) Tailoring water adsorption capacity of APO-Tric, Crystals, 11, 7, article no. 773, 1-12 https://doi.org/10.3390/cryst11070773

[27] Portilla-Nieto, Y., Zaki, A., Vidal, K., Hernaiz, M., Aranzabe, E., Doppiu, S., & Faik, A. (2021). Development of Co3-xNixO4 materials for thermochemical energy storage at lower red-ox temperature. Solar Energy Materials and Solar Cells, 230, 111194. https://doi.org/10.1016/j.solmat.2021.111194

[28] Block, T., Knoblauch, N., & Schmücker, M. (2014). The cobalt-oxide/iron-oxide binary system for use as high temperature thermochemical energy storage material. Thermochimica Acta, 577, 25-32. https://doi.org/10.1016/j.tca.2013.11.025

[29] Mastronardo, E., La Mazza, E., Palamara, D., Piperopoulos, E., Iannazzo, D., Proverbio, E., & Milone, C. (2022). Organic Salt Hydrate as a Novel Paradigm for Thermal Energy Storage. Energies, 15(12), 4339. https://doi.org/10.3390/en15124339

[30] Piperopoulos, E., Fazio, M., Mastronardo, E., Lanza, M., & Milone, C. (2021). Tuning Mg (OH) 2 Structural, Physical, and Morphological Characteristics for Its Optimal Behavior in a Thermochemical Heat-Storage Application. Materials, 14(5), 1091. https://doi.org/10.3390/ma14051091

[31] Fopah-Lele, A., Kuznik, F., Osterland, T., & Ruck, W. K. (2016). Thermal synthesis of a thermochemical heat storage with heat exchanger optimization. Applied Thermal Engineering, 101, 669-677. https://doi.org/10.1016/j.applthermaleng.2015.12.103

[32] Ristić, A., Fischer, F., Hauer, A., & Logar, N. Z. (2018). Improved performance of binder-free zeolite Y for low-temperature sorption heat storage. Journal of Materials Chemistry A, 6(24), 11521-11530. https://doi.org/10.1039/C8TA00827B

[33] Pliekhov, O., Pliekhova, O., Arčon, I., Bondino, F., Magnano, E., Mali, G., Logar, Z. N. (2020). Study of water adsorption on EDTA dealuminated zeolite Y, Microporous Mesoporous Mater. 302, 110208. https://doi.org/10.1016/j.micromeso.2020.110208

[34] Krajnc, A., Varlec, J., Mazaj, M., Ristić, A., Logar, N. Z., & Mali, G. (2017). Superior Performance of Microporous Aluminophosphate with LTA Topology in Solar-Energy Storage and Heat Reallocation. Advanced Energy Materials, 7(11), 1601815. https://doi.org/10.1002/aenm.201601815

[35] Čelič, T.B., Škrjanc, A., Coronado, J.M., Čendak, T., de la Peña O'Shea, V.A., Serrano, D.P., Zabukovec Logar, N. (2022) New Insight into Sorption Cycling Stability of Three Al-Based MOF Materials in Water Vapour, Nanomaterials. 12. https://doi.org/10.3390/nano12122092

[36] Byrne, C., Ristić, A., Mal, S., Opresnik, M., & Zabukovec Logar, N. (2021). Evaluation of ZIF-8 and ZIF-90 as Heat Storage Materials by Using Water, Methanol and Ethanol as Working Fluids. Crystals, 11(11), 1422.
https://doi.org/10.3390/cryst11111422

[37] Nonnen, T.; Beckert, S.; Gleichmann, K.; Brandt, A.; Unger, B.; Kerskes, H.; Mette, B.; Bonk, S.; Badenhop, T.; Salg, F.; et al. (2016**).** A Thermochemical Long-Term Heat Storage System Based on a Salt/Zeolite Composite. Chem. Eng. Technol., 39, 2427–2434.
https://doi.org/10.1002/ceat.201600301

[38] Ristić, A., Zabukovec Logar, N. (2019). New composite water sorbents $CaCl_2$–PHTS for low-temperature sorption heat storage: determination of structural properties. Nanomaterials. 9, 1, 1-16
https://doi.org/10.3390/nano9010027

[39] de Jong, A. J., van Vliet, L., Hoegaerts, C., Roelands, M., & Cuypers, R. (2016). Thermochemical heat storage–from reaction storage density to system storage density. Energy Procedia, 91, 128-137.
https://doi.org/10.1016/j.egypro.2016.06.187

[40] Müller, D., Knoll, C., Gravogl, G., Artner, W., Welch, J. M., Eitenberger, E., ... & Weinberger, P. (2019). Tuning the performance of MgO for thermochemical energy storage by dehydration–From fundamentals to phase impurities. Applied Energy, 253, 113562.
https://doi.org/10.1016/j.apenergy.2019.113562

[41] Shervani, S., Strong, C., & Tezel, F. H. (2022). Magnesium sulphate hybrids with silica gel and activated alumina for thermal energy storage. Journal of Cleaner Production, 371, 133262.
https://doi.org/10.1016/j.jclepro.2022.133262

[42] Ocvirk, M., Ristić, A., & Zabukovec Logar, N. (2021). Synthesis of Mesoporous γ-Alumina Support for Water Composite Sorbents for Low Temperature Sorption Heat Storage. Energies, 14(22), 7809.
https://doi.org/10.3390/en14227809

[43] Kouchachvili, L., Bardy, D. A., Djebbar, R., & Hogg, L. E. (2023). Natural zeolites as host matrices for the development of low-cost and stable thermochemical energy storage materials. Journal of Porous Materials, 30(1), 163-173.
https://doi.org/10.1007/s10934-022-01277-3

[44] Liang, Z., Wang, X., Zhu, W., Zhang, P., Yang, Y., Sun, C., ... & Zhou, L. (2017). Upconversion nanocrystals mediated lateral-flow nanoplatform for in vitro detection. ACS Applied Materials & Interfaces, 9(4), 3497-3504.
https://doi.org/10.1021/acsami.6b14906

[45] Serrano, A., Duran, M., Dauvergne, J. L., Doppiu, S., & Del Barrio, E. P. (2021). Tailored transition temperature plastic crystals with enhanced thermal energy storage capacity. Solar Energy Materials and Solar Cells, 220, 110848.
https://doi.org/10.1016/j.solmat.2020.110848

[46] Serrano, A., Garrido, I., Santos, S., Duran, M., Dauvergne, J. L., Carmona, M., & Del Barrio, E. P. (2022). Effect of processing on microstructure and mechanical properties of

826 pentaglycerine based solid-solid phase change materials. Journal of Energy Storage, 55,
827 105677.
828 https://doi.org/10.1016/J.EST.2022.105677

829 [47] Santos-Moreno, S., Doppiu, S., Lopez, G. A., Marinova, N., Serrano, Á., Silveira, E., &
830 Palomo del Barrio, E. (2020). Study of the phase transitions in the binary system NPG-TRIS
831 for thermal energy storage applications. Materials, 13(5), 1162.
832 https://doi.org/10.3390/ma13051162

833 [48] Mishra, A., Talekar, A., Chandra, D., & Chien, W. M. (2012). Ternary phase diagram
834 calculations of pentaerythritol–pentaglycerine–neopentylglycol system. Thermochimica acta,
835 535, 17-26.
836 https://doi.org/10.1016/j.tca.2012.02.009

837 [49] Barrio, M., Font, J., Muntasell, J., Navarro, J., & Tamarit, J. L. (1988). Applicability for
838 heat storage of binary systems of neopentylglycol, pentaglycerine and pentaerythritol: a
839 comparative analysis. Solar energy materials, 18(1-2), 109-115.
840 https://doi.org/10.1016/0165-1633(88)90051-2

841 [50] Singh, H. (2011). An Experimental Phase Diagram Study of Ternary Pentaerythritol-
842 Pentaglycerine-Neopentylglycol Orieintationally Disordered Plastic Crystals (Doctoral
843 dissertation).
844 https://scholarworks.unr.edu/handle/11714/3912

845 [51] Singh, H., Talekar, A., Chien, W. M., Shi, R., Chandra, D., Mishra, A., & Nelson, D. J.
846 (2015). Continuous solid-state phase transitions in energy storage materials with orientational
847 disorder–Computational and experimental approach. Energy, 91, 334-349.
848 https://doi.org/10.1016/j.energy.2015.07.130

849 [52] Chandra, D., Ding, W., Lynch, R. A., & Tomilinson, J. J. (1991). Phase transitions in
850 “plastic crystals”. Journal of the Less Common Metals, 168(1), 159-167.
851 https://doi.org/10.1016/0022-5088(91)90042-3

852 [53] Gao, W., Lin, W., Liu, T., & Xia, C. (2007). An experimental study on the heat storage
853 performances of polyalcohols NPG, TAM, PE, and AMPD and their mixtures as solid-solid
854 phase-change materials for solar energy applications. International journal of green energy,
855 4(3), 301-311.
856 https://doi.org/10.1080/15435070701332112

857 [54] Shi, R., Chandra, D., Mishra, A., Talekar, A., Tirumala, M., & Nelson, D. J. (2017).
858 Thermodynamic reassessment of the novel solid-state thermal energy storage materials:
859 Ternary polyalcohol and amine system pentaglycerine-tris (hydroxymethyl)-amino-methane-
860 neopentylglycol (PG-TRIS-NPG). Calphad, 59, 61-75.
861 https://doi.org/10.1016/j.calphad.2017.08.003

862 [55] Chandra, D., Chien, W. M., Gandikotta, V., & Lindle, D. W. (2002). Heat capacities of
863 “plastic crystal” solid state thermal energy storage materials. 1443
864 https://doi.org/10.1524/ZPCH.2002.216.12.1433/MACHINEREADABLECITATION/RIS

865 [56] Crespo, A., Frazzica, A., Fernández, C., & de Gracia, Á. (2023). Optimizing the
866 discharge process of a seasonal sorption storage system by means of design and control
867 approach. Journal of Energy Storage, 60, 106652.
868 https://doi.org/10.1016/j.est.2023.106652

[57] Zeng, Z., Zhao, B., & Wang, R. (2022). Water based Adsorption Thermal Battery: Sorption Mechanisms and Applications. Energy Storage Materials. https://doi.org/10.1016/j.ensm.2022.11.024

[58] Donkers, P. A. J., Sögütoglu, L. C., Huinink, H. P., Fischer, H. R., & Adan, O. C. G. (2017). A review of salt hydrates for seasonal heat storage in domestic applications. Applied energy, 199, 45-68. https://doi.org/10.1016/j.apenergy.2017.04.080

[59] Wang, K., Yan, T., Li, R. K., & Pan, W. G. (2022). A review for Ca (OH)2/CaO thermochemical energy storage systems. Journal of Energy Storage, 50, 104612. https://doi.org/10.1016/j.est.2022.104612

[60] Malleswararao, K., & Dutta, P. (2022). Applications of metal hydride based thermal systems: A review. Applied Thermal Engineering, 118816. https://doi.org/10.1016/j.applthermaleng.2022.118816

[61] Bérut, E., Bois, L., Touloumet, Q., Outin, J., Ondarts, M., Postole, G., ... & Le Pierrès, N. (2023). Characterization of silica-PEG-$CaCl_2$ composite sorbents in an open thermochemical heat storage reactor. Journal of Energy Storage, 72, 108632. https://doi.org/10.1016/j.est.2023.108632

[62] Liu, X., Wang, H., Liu, X., Yang, F., Guan, L., Sani, S., ... & Wu, Y. (2022). Development of $MgSO_4$/mesoporous silica composites for thermochemical energy storage: the role of porous structure on water adsorption. Energy Reports, 8, 4913-4921. https://doi.org/10.1016/j.egyr.2022.03.137

[63] Marín, P. E., Milian, Y., Ushak, S., Cabeza, L. F., Grágeda, M., & Shire, G. S. F. (2021). Lithium compounds for thermochemical energy storage: A state-of-the-art review and future trends. Renewable and Sustainable Energy Reviews, 149, 111381. https://doi.org/10.1016/j.rser.2021.111381

[64] Skrylnyk, O., Courbon, E., Heymans, N., Frère, M., Bougard, J., & Descy, G. (2018). Performance characterization of salt-in-silica composite materials for seasonal energy storage design. Journal of Energy Storage 19, 320-336. https://doi.org/10.1016/j.est.2018.08.015

[65] Zhu, D., Wu, H., & Wang, S. (2006). Experimental study on composite silica gel supported $CaCl_2$ sorbent for low grade heat storage. International Journal of Thermal Sciences, 45, 804-813. https://doi.org/10.1016/j.ijthermalsci.2005.10.009

[66] Aristov, Y.I., Restuccia, G., Tokarev, M.M., Cacciola, G. (2000) Selective water sorbents for multiple applications, 10. Energy storage ability. Reaction Kinetics and Catalysis Letters 69, 345-353. https://doi.org/10.1023/A:1005616420331

[67] Steinert, S., Voigt, W., Glausch, R., & Neuschütz, M. (2005). Thermal characteristics of solid–solid phase transitions in long-chain dialkyl ammonium salts. Thermochimica acta, 435(1), 28-33. https://doi.org/10.1016/J.TCA.2005.04.019

911 [68] Font, J., & Muntasell, J. (1995). Comparative study on solid crystalline–plastic–vapour
912 equilibrium in plastic crystals from pentaerythritol series. Journal of Materials Chemistry,
913 5(8), 1137-1140.
914 https://doi.org/10.1039/JM9950501137

915 [69] Barron, A. R. (2010). Determination of Sublimation Enthalpy and Vapor Pressure for
916 Inorganic and Metal-Organic Compounds by Thermogravimetric Analysis. Chemistry of
917 Electronic Materials, OpenStax CNX.

918

919

920

921